# Enhanced interband tunneling in two-dimensional tunneling transistors through anisotropic energy dispersion

Hengze Qu,[1] Shiying Guo,[1] Wenhan Zhou,[1] Zhenhua Wu,[2] Jiang Cao [®],[3] Zhi Li,[1] Haibo Zeng,[1,*] and Shengli Zhang [®][1,†]

[1]*Key Laboratory of Advanced Display Materials and Devices, Ministry of Industry and Information Technology, College of Material Science and Engineering, Nanjing University of Science and Technology, Nanjing 210094, China*

[2]*Key Laboratory of Microelectronics Device and Integrated Technology, Institute of Microelectronics of Chinese Academy of Sciences, Beijing 100029, China*

[3]*School of Electronic and Optical Engineering, Nanjing University of Science and Technology, Nanjing 210094, China*

The unsatisfactory transmission probability in tunneling junction is a major challenge that restricts the performance and scaling of next-generation nanodevices, such as the tunnel field-effect transistors (TFETs). Here, we propose a strategy utilizing anisotropic electronic structures to enhance the inter-band tunneling performance. In the tunneling process, the sharp energy dispersion in transport direction ensures a high transmission eigenvalue, and the weak transverse energy state can broaden the transverse tunneling window, thus strengthening the tunneling probability. Furthermore, our quantum transport simulations demonstrate that in two-dimensional (2D) group VA-VA TFETs, the stronger anisotropic band structures make 2D BiAs and arsenene exhibit high on-state current several times higher than other systems, and the relative larger bandgap of arsenene also gives rise to a steep subthreshold slope below 60 mV/dec. This work provides a physical understanding of the tunneling transport performance, and the anisotropic 2D electronic structures can be regarded as a target feature to design tunneling transistors.

## I. INTRODUCTION

Electron tunneling is a quantum mechanism in which electrons can transmit through the energy barrier [1]. The quantum phenomenon provides new opportunities for the development of advanced modern electronics, such as tunneling field-effect transistors (TFETs) for low-power applications [2]. Taking advantage of the cold injection of band-to-band tunneling mechanism, abruptly switching on and off can be realized in TFETs, which is constructed by reverse-biased *p*-type-intrinsic-*n*-type structures [3,4]. It is possible to break through the Boltzmann tyranny and hence the fundamental subthreshold swing (SS) limits of 60 mV/dec at room temperature in conventional metal-oxide-semiconductor FETs (MOSFETs) [5,6]. However, one challenge in TFETs is to achieve high on-state currents as it critically depends on the transmission probability through the tunnelling barrier [7,8]. Experimentally, increasing the tunneling probability can be realized by exploiting the semiconductors with smaller energy band gaps or heavy doping, which shortens the screening tunneling length. However, these strategies are detrimental to the SS and off-state current [9].

The emergence of exciting electronic properties has been promoting the research upsurge of two-dimensional (2D) electronic materials, such as the electrostatic control capability to alleviate short-channel effects in aggressively scaled electronic devices [10–15]. In particular, the 2D group VA materials [16–18] exhibit physical phenomena and electronic properties, such as high carrier mobility [19–21], anisotropic electronic structure [22–24], Rashba effect [25] and topological states [26,27], which opens a new route to next-generation electronics [28–30].

In this work, we propose a strategy of anisotropic band dispersions to increase on-state current of TFETs, utilizing the puckered 2D group VA monolayers. In the TFETs with anisotropic band structures, the sharp transport energy dispersion can increase the transmission coefficient, and the weak transverse energy state broadens the transverse tunneling window. Specifically, using density functional theory (DFT) coupled with nonequilibrium green's function (NEGF) formalism, we demonstrate that the strong anisotropic electronic structures significantly enhance the on-state current of arsenene and 2D BiAs TFETs. In addition to their moderate band gaps, the SS can be reduced below 60 mV/dec. Furthermore, based on the anisotropic tunneling model, an "intrinsic tunneling factor" ($\bar{T}$) completely determined by electronic structures of 2D semiconductors is defined to search for promising 2D candidates for energy-efficient and high-performance electronic devices.

## II. RESULTS

For 2D materials with anisotropic energy dispersion as shown in Fig. 1(a), the total energy at the band edge can be written as $E = E_{\parallel} + E_{\perp}$ [31], where $E_{\parallel}$ and $E_{\perp}$ are the

*Corresponding author: zeng.haibo@njust.edu.cn
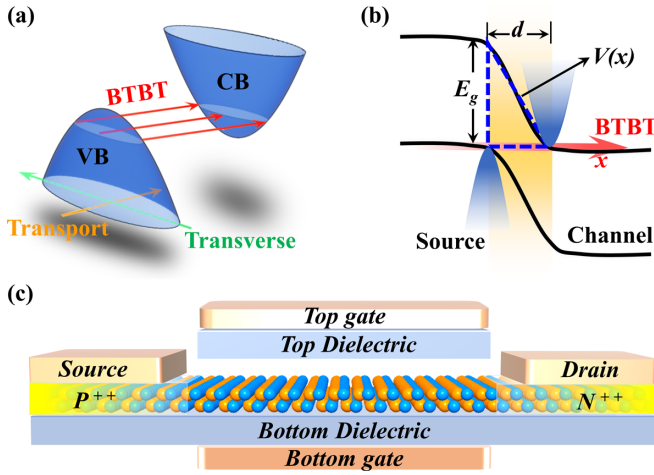†Corresponding author: zhangslvip@njust.edu.cn

FIG. 1. (a) The 3D BTBT schematic diagram between anisotropic valence (VB) and conduction (CB) band edge. (b) Band profile of BTBT in the source-channel junction with the triangular potential barrier model. The red arrows indicate the BTBT process. (c) The device configuration of TFETs.
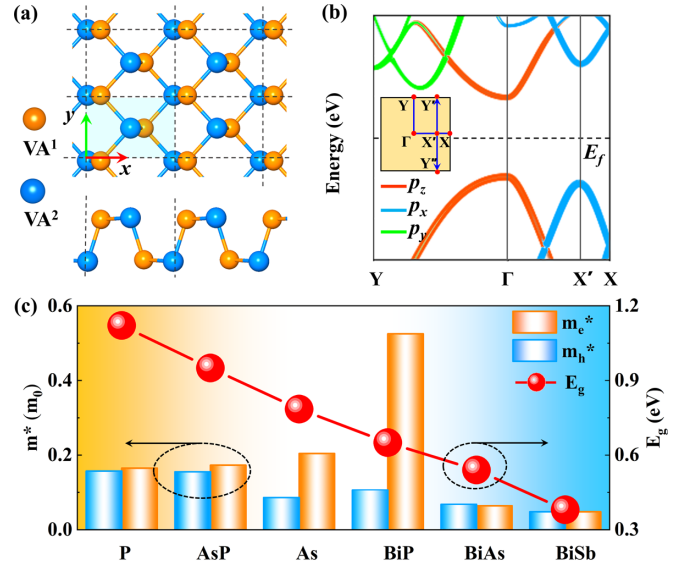


FIG. 2. (a) The geometric structures and (b) the orbital projected band structure sketch of 2D group VA monolayers. The inset represents the first Brillouin zone. $VA^1$ and $VA^2$ represent two kinds of group-VA elements. (c) Band gap ($E_g$) and effective mass of electron ($m_e^*$, orange) and hole ($m_h^*$, blue) along the armchair direction for group VA monolayers.

energy in transport direction and transverse directions, respectively. In the band-to-band tunneling process, parabolic energy dispersion in transport direction can be expressed by $E_\parallel = \frac{\hbar^2 k_\parallel^2}{2m_\parallel^*}$. Based on a triangular potential barrier model shown in Fig. 1(b), the potential profile in the tunneling window can be written by $V(x) = E + q\xi x$, where $q\xi$ is electric field. The wave vector $k_\parallel(x)$ in the tunneling region can be written as (see Appendix A):

$$k_\parallel(x) = \left[ \frac{2m_\parallel^*}{\hbar^2} \left( -\frac{\hbar^2 k_\perp^2}{2m_\perp^*} - q\xi x \right) \right]^{\frac{1}{2}}. \quad (1)$$

According to the Wentzel-Kramer-Brillouin (WKB) approximation, as the width of the tunneling window can be defined by the band gap $E_g$ and electric field q$\xi$, $d = E_g/q\xi$. The tunneling probability can be expressed by [2,32]

$$T = e^{-\alpha}, \quad \alpha = \frac{4(2m_\parallel^*)^{\frac{1}{2}} \left( E_g + \frac{\hbar^2 k_\perp^2}{2m_\perp^*} \right)^{\frac{3}{2}}}{3q\hbar\xi}. \quad (2)$$

Equation (2) suggests that, except from light transport effective mass $m_\parallel^*$ and small band gap $E_g$, decreasing the trasverse energy $E_\perp$ through increasing the transverse effective mass $m_\perp^*$ is also beneficial to improve the tunneling probabilities. The band-to-band tunneling is the fundamental working mechanism of TFETs, which is constructed as reverse-biased $p$-type-intrinsic-$n$-type structures, as shown in Fig. 1(c). Therefore, anisotropic energy dispersion is necessary to pursue high tunneling current for TFETs.

2D group VA monolayers like black phosphorene share puckered honeycomb configuration, as shown in Fig. 2(a), which reduces the $D_{6h}$ symmetry of planar hexagonal honeycomb (like that in graphene) to $D_{2h}$. Therefore, their electronic structures exhibit an anisotropic characteristic. Besides, as shown in Fig. 2(b), they also exhibit multivalleys with $p$-orbital symmetry around the fermi level.

For black phosphorene, the valence band maximum (VBM) and conduction band minimum (CBM) are at $\Gamma$ point, forming a direct bandgap semiconductor. With the atomic weight increasing, the Coulomb repulsion from the nonbonding shells weakens the orbital overlapping and the $sp$ hybridization strength, increasing the energy of the $X'$ valley at VB. Therefore, for AsP monolayer, the energy difference between $\Gamma$ and $X'$ valley is smaller than that in black phosphorene. In addition, for black arsenene, the energy of the $p_x$-dominated $X'$ valley exceeds that of $\Gamma$ valley, forming an indirect band gap (see Fig. S1 in the Supplemental Material [33]).

For BiP, BiAs, and BiSb monolayers, the ultralarge radius of Bi atoms leads to a distorted washboard structure (see Fig. S2 in the Supplemental Material [33]) with broken inversion symmetry ($C_{2v}$ symmetry). The weaker $sp$ hybridization decreases the splitting between bonding and antibonding states, causing smaller band gaps. For 2D BiP, the band structure is like arsenene with the band gap reduced to 0.61 eV, while for 2D BiAs and BiSb, both the VBM and CBM shift to $X'$ point with the band gap of 0.53 and 0.38 eV, respectively (see Fig. S3 in the Supplemental Material [33]).

The decreasing trend of band gap from phosphorene, AsP, arsenene, BiP, BiAs, to BiSb (from 1.12 to 0.38 eV) is summarized in Fig. 2(c). Furthermore, the electron and hole effective masses along armchair direction indicates that almost all the values are smaller than that of 2D transition metal dichalcogenides (the effective mass for $MoS_2$, $MoSe_2$ and $WSe_2$ ranges $0.44 \sim 0.61\,m_0$).

In this view, we evaluate and test the potential benefit to the tunneling current based on these 2D group VA monolayers. We first present a comparative analysis of 2D BiAs and
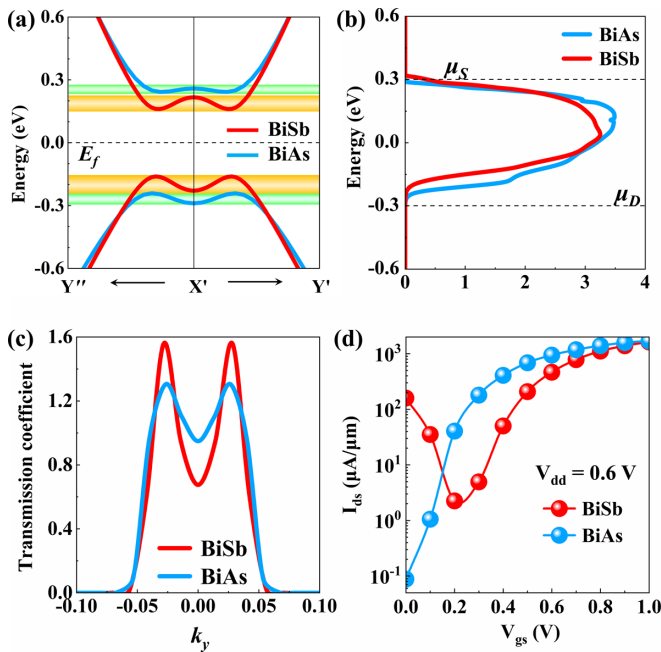
FIG. 3. (a) The energy band dispersion of 2D BiAs and BiSb monolayers along zigzag direction in first Brillouin zone. The width of green and orange ribbons broadening of the M-type band edge. The Fermi level is set to zero. (b) Transmission spectrum of 2D BiAs and BiSb, as $V_{gs}$ is 0.8 V and $V_{dd}$ is 0.6 V, two black dashed lines top and bottom represent the Fermi level of the source $\mu_S$ and drain $\mu_D$, respectively. (c) The transmission coefficient of 2D BiAs and BiSb TFETs along the transverse direction in momentum space. (d) Transfer characteristics of 2D BiAs and BiSb TFETs with 12-nm channel.



FIG. 4. (a) The transmission coefficient along the transverse direction in the momentum space. (b)Transfer characteristics of 2D BiP and arsenene TFETs. (c) Minimum leakage current ($I_{min}$) of the group VA monolayer TFETs as a function of band gap ($E_g$). The blue line is the fitting function $I_{min} = A \exp(-B \times E_g)$, where $A$ and $B$ are constants of 272.56 and 16.95, respectively. (d) On-state current ($I_{on}$) of group VA monolayer TFETs varies with the band gap ($E_g$), as the off-current is fixed at 0.1 $\mu A/\mu m$.

BiSb, since these two systems share the similar electronic band structures with the band edge located at the $X'$ point [34]. However, 2D BiSb shows a smaller $E_g$ and sharp energy dispersions compared with 2D BiAs. The $E_g$ is 0.38 eV versus 0.56 eV, while the reduced effective mass in armchair direction is 0.048 $m_0$ versus 0.065 $m_0$. As shown in Fig. 3(a), different from that in armchair direction, their energy dispersion along zigzag direction ($Y'' \to X' \to Y'$ path) presents an M-type quartic dispersion, and that of 2D BiAs is much weaker than that of 2D BiSb (Note S1 and Fig. S4 in the Supplemental Material [33]).

Figure 3(b) shows the tunneling transmission spectrums of 2D BiSb and BiAs TFETs, and the simulated projected local density of states (PLDOS) is shown in Fig. S5 in the Supplemental Material [33]. Specifically, the device structure is shown in Fig. 1(c). The armchair orientation is selected as the transport direction. A 12-nm channel is covered by the gate oxide layer with equivalent oxide thickness of 0.5 nm, and supply voltage $V_{dd}$ of 0.6V, according to the criteria of International Roadmap of Devices and Systems (IRDS) in 2031 horizon [35]. For both 2D BiAs and BiSb TFETs the p-doped source concentrations is $1 \times 10^{13}$ cm$^{-2}$ and n-doped drain concentration is $1 \times 10^{12}$ cm$^{-2}$. Clearly, one notes that 2D BiAs exhibits higher transmission eigenvalues than 2D BiSb in the bias window, as their maximum values are 0.105 versus 0.097, respectively. The trend of the
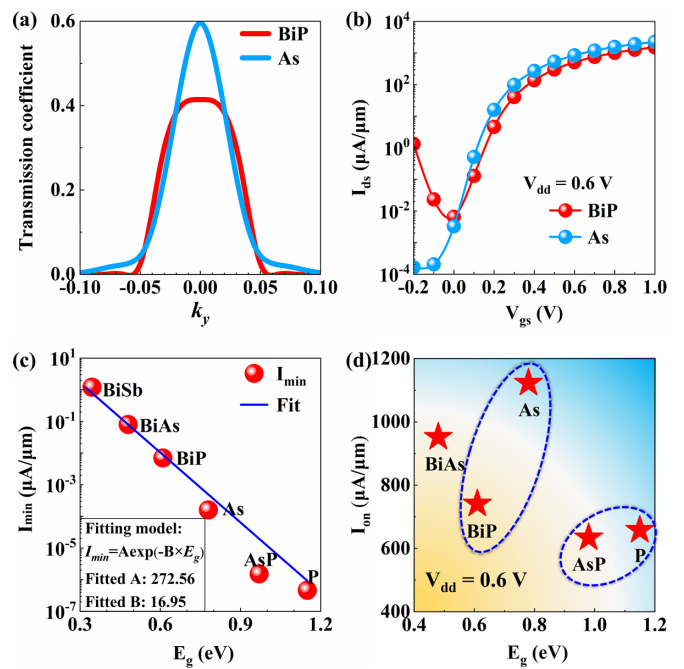
transmission eigenvalues between 2D BiAs and BiSb can be described using the transmission coefficient of electronic state, as illustrated in Fig. 3(c). Due to the weaker transverse energy dispersion, 2D BiAs has more tunneling states at the same energy level, resulting in a larger transmission eigenstate than 2D BiSb. Therefore, the current in threshold region of 2D BiAs TFETs is higher than that of 2D BiSb [Fig. 3(d)]. Similarly, the weaker transverse energy dispersion of black phosphorene also leads to a higher tunneling current than that of 2D AsP (Figs. S6 and S7 in the Supplemental Material [33]).

It is also interesting to compare the transport performances of 2D BiP TFETs to that of arsenene (the p-doped source concentration is $5 \times 10^{13}$ cm$^{-2}$ and n-doped drain concentration is $1 \times 10^{12}$ cm$^{-2}$), as the band edges of these two systems are located at the same positions. 2D BiP possesses slightly weaker transverse energy dispersion of the valence band edge than arsenene (Fig. S8 in the Supplemental Material [33]). However, the electron and hole effective masses in the transport direction for arsenene are 0.20 and 0.08 $m_0$, which are much lighter than those of 2D BiP (0.53 $m_0$ for electron and 0.11 $m_0$ for hole), which leads to arsenene a sharper peak than 2D BiP in the transmission coefficient as illustrated in Fig. 4(a). The trend of their corresponding transmission spectrum and their PLDOS are shown in Figs. S9 and S10 of the Supplemental Material [33]. Therefore, the saturation current of arsenene is much higher than that 2D BiP, that is 1553 $\mu A/\mu m$ versus 1012 $\mu A/\mu m$ [Fig. 4(b)]. In this view,
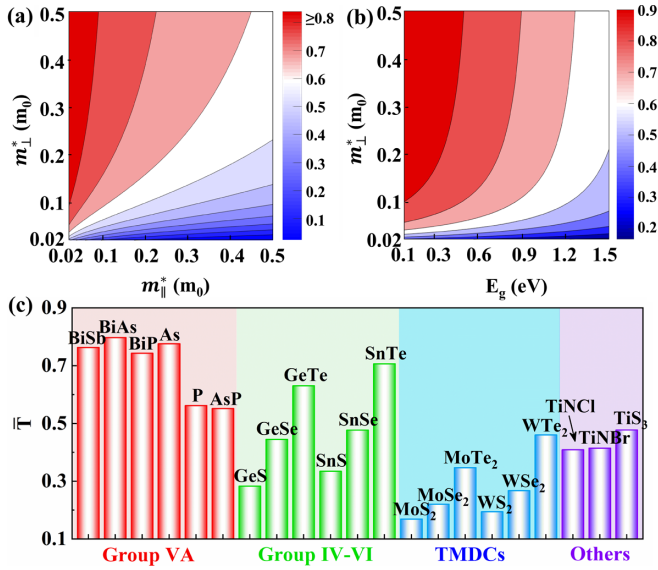
FIG. 5. (a) Intrinsic tunneling coefficient $\bar{T}$ as a function of $m_\perp^*$ and $m_\parallel^*$, as the $E_g$ is 0.6 eV. (b) $\bar{T}$ as a function of $m_\perp^*$ and $E_g$, as the $m_\parallel^*$ is 0.05 $m_0$. (c) The calculated intrinsic tunneling coefficient of different groups of 2D semiconductors.

a stronger anisotropic band edge dispersion is more beneficial to obtain a large tunneling current.

The on-state current of FETs is determined by $V_{dd} = |V_{gs/on} - V_{gs/off}|$ ($V_{gs/off}$ is the gate voltage corresponding to the $I_{off}$, $V_{gs/on}$ is the gate voltage corresponding to $I_{on}$, and $V_{dd}$ is the supply voltage). Before evaluating the on-state current, the leakage current and the switching capability should be tested due to the generally ambipolar behavior in TFETs [36]. As shown in Figs. 4(c) and S11 in the Supplemental Material [33], the minimum leakage current and SS of the above six systems decrease as functions of band gap $E_g$, which can be quantified by the exponential fit, $y = A \exp(-B \times E_g)$. Fig. 4(d) shows the on-state current for 2D group VA TFETs with the $I_{off}$ fixed at 0.1 $\mu A/\mu m$ (since the minimum leakage current of 2D BiSb TFET cannot be reduced below 0.1 $\mu A/\mu m$, its on-state current cannot be evaluated, see Note S2 and Fig. S12 in the Supplemental Material [33]). The 2D BiAs has an on-state current of 962 $\mu A/\mu m$. Specifically, we find a high on-state current of 1123 $\mu A/\mu m$ for arsenene TFET, much higher than the that of 2D BiP TFET (741 $\mu A/\mu m$). For the phosphorene TFET, its on-state current is 658 $\mu A/\mu m$, but still higher than that of 2D AsP (602 $\mu A/\mu m$).

To universally evaluate the tunneling behavior of semiconductor materials, we further extract the correlate parameters of electronic structures from Eq. (2) and define a "intrinsic tunneling factor" ($\bar{T}$) of 2D semiconductors as

$$\bar{T} = e^{-\beta}, \quad \beta = (m_\parallel^*)^{\frac{1}{2}} \left( E_g + \frac{\hbar^2 k_\perp^2}{2 m_\perp^*} \right)^{\frac{3}{2}}. \quad (3)$$

Figure 5(a) shows the variation of $\bar{T}$ of the 2D materials as a funtion of $m_\perp^*$ and $m_\parallel^*$. The high $\bar{T}$ tends to range in the left-upper regions which show anisotropic effective mass. In addition, the values of $\bar{T}$ as a function of $E_g$ respectively

considering $m_\perp^*$ and $m_\parallel^*$ are plotted in Fig. 5(b) and Fig. S13 in the Supplemental Material [33]. A heavy $m_\perp^*$ and a light $m_\parallel^*$ can effectively suppress the adverse effect of the increase of $E_g$ on tunneling current. Therefore, an anisotropic 2D semiconductors with moderate $E_g$ could decouple the increase in leakage current and SS from the increase in on-state current.

We further calculate the values of $\bar{T}$ of the group VA monolayers and compare them with other 2D materials, as shown in Fig. 5(c). We find that the values of $\bar{T}$ for 2D BiAs is 0.75, higher than that for 2D BiSb ($\bar{T} = 0.67$). Moreover, the values of $\bar{T}$ for arsenene is 0.76, higher than that for BiP ($\bar{T} = 0.63$), and those for P and AsP are 0.56 and 0.55, respectively. In addition, the values of $\bar{T}$ for 2D GeTe and SnTe are comparable with that of group VA monolayers. Except for the high $\bar{T}$, they also have moderate $E_g$, as shown in Fig. S14 in the Supplemental Material [33], which are sufficient for achieving small off-state current and steep SS.

In addition to channel transport, charge injection through electrical contacting 2D semiconductor is also an inevitable process for 2D electronic devices [37]. The interface charge injection includes two distinct contact configurations, namely the vertical heterostructure and the lateral heterostructure. For both lateral and vertical heterostructure contacts, the saturation current density is demonstrated to be proportional to the effective mass and DOS [38]. The anisotropic 2D materials possess the heavier effective mass in the $y$ direction than that in the $x$ direction, which results in a larger in-plane effective mass m* than the isotropic 2D materials. Therefore, for the interfacial charge injection through 2D electrical contacts, the anisotropic band structure also has potential to obtain a high thermionic current.

## III. METHODS

The simulations of electronic and quantum transport properties of 2D group VA materials are performed by the Quantum Atomistix Toolkit (ATK) package [39]. For all 2D group VA models, a vacuum thickness of 40 Å in $z$ orientation is used for eliminating the periodicity, and the Perdew-Burke-Ernzerhof (PBE) function of general gradient-corrected (GGA) are used to deal with the exchange-correlation potential [40,41]. For geometry optimization, the tolerances for force and the stress error are $1.0 \times 10^{-4}$ eV and 0.01 eV/Å, respectively. The density mesh cutoff is 105 Ha and Monkhorst-Pack $k$ meshes is $12 \times 10 \times 1$.

The quantum transport performances are simulated based on DFT coupled with NEGF formalism [42], and GGA-PBE functions are used. The driven current $I_{ds}$ at certain $V_{dd}$ and $V_g$ are calculated by the Landauer-Büttiker formula [43]:

$$I_{ds}(V_{dd}, V_g) = \frac{2e}{h} \int_{-\infty}^{+\infty} \{ T(E)[f(E - \mu_s) - f(E - \mu_d)] \} dE, \quad (4)$$

where $f(E)$ represents the Fermi-Dirac distribution function, $\mu_{s/d}$ correponds to the electrochemical potential for the source/drain electrode and $T(E)$ is the transmission coefficient. The basis set of double-zeta plus polarization with the density mesh cutoff of 105 Ha was adopted. The $k$-point sampling is $50 \times 1 \times 100$. The electrode temperature is set as 300 K.

## IV. CONCLUSIONS

In summary, we introduce a simple anisotropic electronic structure for improving the on-state current of 2D TFETs, which not only leads to a high transmission eigenvalue in transport direction, but also broadens the transverse transmission window. Furthermore, since the ambipolar leakage current and SS decrease exponentially with the band gap, we propose that 2D semiconductors with a strong anisotropic energy dispersion and a relatively large band gap exhibit superior switching capability and performance. Especially, arsenene TFET presents a high on-state current above $10^3\ \mu A/\mu m$ with a small SS of 46 mV/dec. Uncovering a physical understanding of the operation mechanism between 2D band structure and tunneling behavior, our work provides a general guidance for design of the next-generation nanoelectronic devices based on quantum mechanical band-to-band tunneling effect.

## APPENDIX A: TUNNELING OF PARABOLIC ANISOTROPIC DISPERSION

According to the WKB approximation, the tunneling probability $T$ can be described by the equation

$$T = \exp\left(-2\int |k_\parallel(x)|dx\right). \quad (A1)$$

$k_\parallel(x)$ is the wave vector in the tunneling region. For 2D semiconductors, the effective mass along the tunneling direction is denoted by $m_\parallel^*$, while that along the direction perpendicular to tunneling direction is denoted by $m_\perp^*$. Therefore, the total energy in the tunneling region can be written as

$$E = \frac{\hbar^2 k_\parallel^2}{2m_\parallel^*} + \frac{\hbar^2 k_\perp^2}{2m_\perp^*}, \quad (A2)$$

where $\hbar$ is the reduced Planck constant, $k_\perp$ is the wave vector perpendicular to the tunneling direction. As the interband tunneling includes the electron states of valence band and conduction band, the reduced carrier effective mass $m_\parallel^*$ and $m_\perp^*$ are defined as $(\frac{1}{m_e^*} + \frac{1}{m_h^*})^{-1}$. Based on a triangular potential barrier model, the wave vector $k_\parallel(x)$ in the tunnelling region is expressed as

$$k_\parallel(x) = \left[\frac{2m_\parallel^*}{\hbar^2}(E_\parallel - V(x))\right]^{\frac{1}{2}}. \quad (A3)$$

The potential profile of the tunneling window $V(x)$ can be written by $V(x) = E + q\xi x$, where $q\xi$ is electric field potential. Therefore, the wave vector in the tunneling region can be written as

$$k_\parallel(x) = \left[\frac{2m_\parallel^*}{\hbar^2}(-E_\perp - q\xi x)\right]^{\frac{1}{2}}. \quad (A4)$$

## APPENDIX B: TUNNELING OF SEMI-DIRAC ENERGY DISPERSION

For 2D anisotropic semiconductors, such as multilayer black phosphorus [44], the energy dispersion could dispersion quadratically in one direction and linearly in the orthogonal direction [45]. Thus, we further make a discussion for this kind of condition.

For the linear energy dispersion in the transport direction, the corresponding energy can be denoted as $E_\parallel = \hbar v_F k_\parallel$, where $v_F$ is the Fermi velocity. For the parabolic energy dispersion in the transverse direction, the energy is defined as $E_\perp = \frac{\hbar^2 k_\perp^2}{2m_\perp^*}$. Therefore, the wave vector $k_\parallel(x)$ in the tunnelling region can be written as

$$k_\parallel(x) = \frac{-E_\perp - q\xi x}{\hbar v_F}. \quad (B1)$$

Taking Eq. (B1) into Eq. (A1), the tunneling probability $T$ can be expressed by

$$T = e^{-\gamma}, \quad \gamma = \frac{E_g(E_g + 2E_\perp)}{2\hbar q\xi v_F}. \quad (B2)$$

Further extracting the correlate parameters of electronic structures from Eq. (B2), we can obtain the "intrinsic tunneling factor" ($\bar{T}$):

$$\bar{T} = e^{-\delta}, \quad \delta = \frac{E_g\left(E_g + \frac{\hbar^2 k_\perp^2}{2m_\perp^*}\right)}{2\hbar v_F}. \quad (B3)$$

[1] C. Zener and R. H. Fowler, A theory of the electrical breakdown of solid dielectrics, Proc. R. Soc. London Ser. A **145**, 523 (1934).

[2] A. C. Seabaugh and Q. Zhang, Low-voltage tunnel transistors for beyond CMOS logic, Proc. IEEE **98**, 2095 (2010).

[3] A. M. Ionescu and H. Riel, Tunnel field-effect transistors as energy-efficient electronic switches, Nature (London) **479**, 329 (2011).

[4] C. Gong, H. Zhang, W. Wang, L. Colombo, R. M. Wallace, and K. Cho, Band alignment of two-dimensional transition metal dichalcogenides: Application in tunnel field effect transistors, Appl. Phys. Lett. **103**, 053513 (2013).

[5] J. Appenzeller, Y. M. Lin, J. Knoch, and P. Avouris, Band-to-Band Tunneling in Carbon Nanotube Field-Effect Transistors, Phys. Rev. Lett. **93**, 196805 (2004).

[6] D. Sarkar, X. Xie, W. Liu, W. Cao, J. Kang, Y. Gong, S. Kraemer, P. M. Ajayan, and K. Banerjee, A subthermionic tunnel field-effect transistor with an atomically thin channel, Nature (London) **526**, 91 (2015).

[7] R. J. Prentki, M. Harb, L. Liu, and H. Guo, Nanowire Transistors with Bound-Charge Engineering, Phys. Rev. Lett. **125**, 247704 (2020).

[8] C. Qiu, F. Liu, L. Xu, B. Deng, M. Xiao, J. Si, L. Lin, Z. Zhang, J. Wang, H. Guo, H. Peng, and L.-M. Peng, Dirac-source field-effect transistors as energy-efficient, high-performance electronic switches, Science **361**, 387 (2018).

[9] H. Lu and A. Seabaugh, Tunnel field-effect transistors: State-of-the-art, IEEE J. Electron. Dev. Soc. **2**, 44 (2014).

[10] K. S. Novoselov, A. Mishchenko, A. Carvalho, and A. H. Castro Neto, 2D materials and van der Waals heterostructures, Science **353**, aac9439 (2016).

[11] G. Fiori, F. Bonaccorso, G. Iannaccone, T. Palacios, D. Neumaier, A. Seabaugh, S. K. Banerjee, and L. Colombo, Electronics based on two-dimensional materials, Nat. Nanotechnol. **9**, 768 (2014).

[12] J. Lyu, J. Pei, Y. Guo, J. Gong, and H. Li, A new opportunity for 2D van der Waals heterostructures: Making steep-slope transistors, Adv. Mater. **32**, 1906000 (2020).

[13] Y. Liu, N. O. Weiss, X. Duan, H.-C. Cheng, Y. Huang, and X. Duan, van der Waals heterostructures and devices, Nat. Rev. Mater. **1**, 16042 (2016).

[14] Y. Wang, S. Liu, Q. Li, R. Quhe, C. Yang, Y. Guo, X. Zhang, Y. Pan, J. Li, H. Zhang, L. Xu, B. Shi, H. Tang, Y. Li, J. Yang, Z. Zhang, L. Xiao, F. Pan, and J. Lu, Schottky barrier heights in two-dimensional field-effect transistors: From theory to experiment, Rep. Prog. Phys. **84**, 056501 (2021).

[15] C. Liu, H. Chen, S. Wang, Q. Liu, Y.-G. Jiang, D. W. Zhang, M. Liu, and P. Zhou, Two-dimensional materials for next-generation computing technologies, Nat. Nanotechnol. **15**, 545 (2020).

[16] S. Zhang, Z. Yan, Y. Li, Z. Chen, and H. Zeng, Atomically thin arsenene and antimonene: Semimetal–semiconductor and indirect–direct band-gap transitions, Angew. Chem. Int. Ed. **54**, 3112 (2015).

[17] S. Guo, Y. Zhang, Y. Ge, S. Zhang, H. Zeng, and H. Zhang, 2D V-V binary materials: Status and challenges, Adv. Mater. **31**, 1902352 (2019).

[18] S. Zhang, M. Xie, F. Li, Z. Yan, Y. Li, E. Kan, W. Liu, Z. Chen, and H. Zeng, Semiconducting group 15 monolayers: A broad range of band gaps and high carrier mobilities, Angew. Chem. Int. Ed. **55**, 1666 (2016).

[19] L. Cheng, C. Zhang, and Y. Liu, The optimal electronic structure for high-mobility 2D semiconductors: Exceptionally high hole mobility in 2D antimony, J. Am. Chem. Soc. **141**, 16296 (2019).

[20] G. Pizzi, M. Gibertini, E. Dib, N. Marzari, G. Iannaccone, and G. Fiori, Performance of arsenene and antimonene double-gate MOSFETs from first principles, Nat. Commun. **7**, 12585 (2016).

[21] L. Cheng, C. Zhang, and Y. Liu, Why Two-Dimensional Semiconductors Generally have Low Electron Mobility, Phys. Rev. Lett. **125**, 177701 (2020).

[22] J. Qiao, X. Kong, Z.-X. Hu, F. Yang, and W. Ji, High-mobility transport anisotropy and linear dichroism in few-layer black phosphorus, Nat. Commun. **5**, 4475 (2014).

[23] H. Qu, S. Guo, W. Zhou, and S. Zhang, Uncovering the anisotropic electronic structure of 2D group VA-VA monolayers for quantum transport, IEEE Electron. Device. Lett. **42**, 66 (2021).

[24] S. Zhao, E. Wang, E. A. Üzer, S. Guo, R. Qi, J. Tan, K. Watanabe, T. Taniguchi, T. Nilges, P. Gao, Y. Zhang, H.-M. Cheng, B. Liu, X. Zou, and F. Wang, Anisotropic moiré optical transitions in twisted monolayer/bilayer phosphorene heterostructures, Nat. Commun. **12**, 3947 (2021).

[25] K. Wu, J. Chen, H. Ma, L. Wan, W. Hu, and J. Yang, Two-dimensional giant tunable Rashba semiconductors with two-atom-thick buckled honeycomb structure, Nano Lett. **21**, 740 (2021).

[26] S. Zhang, W. Zhou, Y. Ma, J. Ji, B. Cai, S. A. Yang, Z. Zhu, Z. Chen, and H. Zeng, Antimonene oxides: Emerging tunable direct bandgap semiconductor and novel topological insulator, Nano Lett. **17**, 3434 (2017).

[27] M. Nadeem, I. Di Bernardo, X. Wang, M. S. Fuhrer, and D. Culcer, Overcoming Boltzmann's tyranny in a transistor via the topological quantum field effect, Nano Lett. **21**, 3155 (2021).

[28] M. Long, A. Gao, P. Wang, H. Xia, C. Ott, C. Pan, Y. Fu, E. Liu, X. Chen, W. Lu, T. Nilges, J. Xu, X. Wang, W. Hu, and F. Miao, Room temperature high-detectivity mid-infrared photodetectors based on black arsenic phosphorus, Sci. Adv. **3**, e1700589 (2017).

[29] N. H. D. Khang, Y. Ueda, and P. N. Hai, A conductive topological insulator with large spin Hall effect for ultralow power spin–orbit torque switching, Nat. Mater. **17**, 808 (2018).

[30] M. Zhong, Q. Xia, L. Pan, Y. Liu, Y. Chen, H.-X. Deng, J. Li, and Z. Wei, Thickness-dependent carrier transport characteristics of a new 2D elemental semiconductor: Black arsenic, Adv. Funct. Mater. **28**, 1802581 (2018).

[31] J. Cao, Y. Wu, H. Zhang, D. Logoteta, S. Zhang, and M. Pala, Dissipative transport and phonon scattering suppression via valley engineering in single-layer antimonene and arsenene field-effect transistors, npj 2D Mater. Appl. **5**, 59 (2021).

[32] D. J. Griffiths and D. F. Schroeter, *Introduction to Quantum Mechanics* (Cambridge University Press, Cambridge, 2018).

[33] See Supplemental Material at http://link.aps.org/supplemental/10.1103/PhysRevB.105.075413 for details of band structures, transmission spectrum, projected local density of states, spectrum current, and intrinsic tunneling factor.

[34] S. Guo, W. Zhou, B. Cai, K. Zhang, S. Zhang, and H. Zeng, Band engineering realized by chemical combination in 2D group VA–VA materials, Nanoscale Horiz. **4**, 1145 (2019).

[35] International Roadmap for Devices and Systems, 2020 edition. https://irds.ieee.org/editions/2020.

[36] D. B. Abdi and M. J. Kumar, Controlling ambipolar current in tunneling FETs using overlapping gate-on-drain, IEEE J. Electron Dev. Soc. **2**, 187 (2014).

[37] Y. S. Ang, L. Cao, and L. K. Ang, Physics of electron emission and injection in two-dimensional materials: Theory and simulation, InfoMat **3**, 502 (2021).

[38] Y. S. Ang, H. Y. Yang, and L. K. Ang, Universal Scaling Laws in Schottky Heterostructures Based on Two-Dimensional Materials, Phys. Rev. Lett. **121**, 056802 (2018).

[39] S. Smidstrup, T. Markussen, P. Vancraeyveld, J. Wellendorff, J. Schneider, T. Gunst, B. Verstichel, D. Stradi, P. A. Khomyakov, U. G. Vej-Hansen, M.-E. Lee, S. T. Chill, F. Rasmussen, G. Penazzi, F. Corsetti, A. Ojanperä, K. Jensen, M. L. N. Palsgaard,

U. Martinez, A. Blom, M. Brandbyge, and K. Stokbro, QuantumATK: An integrated platform of electronic and atomic-scale modelling tools, J. Phys.: Condens. Matter. **32**, 015901 (2019).

[40] J. P. Perdew, K. Burke, and M. Ernzerhof, Generalized Gradient Approximation Made Simple, Phys. Rev. Lett. **77**, 3865 (1996).

[41] M. J. van Setten, M. Giantomassi, E. Bousquet, M. J. Verstraete, D. R. Hamann, X. Gonze, and G. M. Rignanese, The PseudoDojo: Training and grading a 85 element optimized norm-conserving pseudopotential table, Comput. Phys. Commun. **226**, 39 (2018).

[42] M. Brandbyge, J.-L. Mozos, P. Ordejón, J. Taylor, and K. Stokbro, Density-functional method for nonequilibrium electron transport, Phys. Rev. B **65**, 165401 (2002).

[43] S. Datta and H. van Houten, Electronic transport in mesoscopic systems, Phys. Today. **49**, 70 (1996).

[44] T. Low, A. S. Rodin, A. Carvalho, Y. Jiang, H. Wang, F. Xia, and A. H. Castro Neto, Tunable optical properties of multilayer black phosphorus thin films, Phys. Rev. B **90**, 075434 (2014).

[45] Y. S. Ang, S. A. Yang, C. Zhang, Z. Ma, and L. K. Ang, Valleytronics in merging Dirac cones: All-electric-controlled valley filter, valve, and universal reversible logic gate, Phys. Rev. B **96**, 245410 (2017).